J Mater Sci: Mater Med (2009) 20:883–888
DOI 10.1007/s10856-008-3661-5

A study of the formation of amorphous calcium phosphate and hydroxyapatite on melt quenched Bioglass® using surface sensitive shallow angle X-ray diffraction

R. A. Martin · H. Twyman · D. Qiu · J. C. Knowles · R. J. Newport

Received: 15 September 2008 / Accepted: 1 December 2008 / Published online: 13 December 2008

Abstract Melt quenched silicate glasses containing calcium, phosphorous and alkali metals have the ability to promote bone regeneration and to fuse to living bone. These glasses, including 45S5 Bioglass® [$(CaO)_{26.9}(Na_2O)_{24.4}(SiO_2)_{46.1}(P_2O_5)_{2.6}$], are routinely used as clinical implants. Consequently there have been numerous studies on the structure of these glasses using conventional diffraction techniques. These studies have provided important information on the atomic structure of Bioglass® but are of course intrinsically limited in the sense that they probe the bulk material and cannot be as sensitive to thin layers of near-surface dissolution/growth. The present study therefore uses surface sensitive shallow angle X-ray diffraction to study the formation of amorphous calcium phosphate and hydroxyapatite on Bioglass® samples, pre-reacted in simulated body fluid (SBF). Unreacted Bioglass® is dominated by a broad amorphous feature around 2.2 $Å^{-1}$ which is characteristic of sodium calcium silicate glass. After reacting Bioglass® in SBF a second broad amorphous feature evolves $\sim$1.6 $Å^{-1}$ which is attributed to amorphous calcium phosphate. This feature is evident for samples after only 4 h reacting in SBF and by 8 h the amorphous feature becomes comparable in magnitude to the background signal of the bulk Bioglass®. Bragg peaks characteristic of hydroxyapatite form after 1–3 days of reacting in SBF.

R. A. Martin (✉) · H. Twyman · D. Qiu · R. J. Newport
School of Physical Sciences, University of Kent,
Ingram Building, Canterbury, Kent CT2 7NH, UK
e-mail: R.A.Martin@Kent.ac.uk

J. C. Knowles
Division of Biomaterials and Tissue Engineering,
Eastman Dental Institute, University College London,
256 Gray's Inn Road, London WC1X 8LD, UK

1 Introduction

Bioactive glasses are of great importance due to their ability to bond to bone and stimulate new bone growth [1, 2]. Their regenerative potential has been demonstrated in clinical trials [3] and Bioglass®, which has been in clinical use since 1985 [4], has already been used in over half a million cases. Bioglass®, also known as 45S5, was the first composition developed and is now sold commercially under the brand names PerioGlass®, Novabone® and NovaBone-C/M® [5].

Bioglass® 45S5, first reported by Hench and coworkers in 1971 [1], consists of 45% (by weight) SiO_2, 24.5% CaO 24.5% Na_2O, 6% P_2O_5. The low % of SiO_2 and correspondingly low network connectivity is essential for the dissolution of elements from the glass. Compositions with greater than 60% weight SiO_2 are bio-inert and those with between 52–60% by weight SiO_2 exhibit slower bonding rates. The release of calcium during the dissolution of these bioactive glasses is thought to be the first step in the mechanism of glass dissolution and formation of the hydroxy calcium apatite (HCA) surface layer, probably via cation exchange between the glass (Ca^{2+} ions) and the simulated body fluid, SBF (H^+ or H_3O^+). Solid state NMR and X-ray diffraction data shows that the dissolution of calcium from the glass (and more slowly, the dissolution of the silica) is associated with the growth of minerals onto and within the porous glass. The formation of a disordered polycrystalline calcium phosphate phase is followed by more ordered calcium phosphates and ultimately a disordered hydroxyapatite phase which eventually crystallises. There are a large number of calcium phosphate phases as described by Dorozhkin and Epple [6], recent evidence suggests that octacalcium phosphate is the preferred

intermediate state deposited prior to the formation of disordered HA [7].

Significant progress has been made on understanding the local atomic scale structure of Bioglass® by employing a range of techniques including NMR [8], neutron diffraction [9] and high energy X-ray diffraction [10, 11]. These techniques provide excellent information on the bulk structure of the glass, but are of course intrinsically limited in the sense that it cannot be as sensitive to thin layers of near-surface dissolution/growth.

Here we specifically investigate the surface structure of flat-plate Bioglass® samples pre-reacted in simulated body fluid at 37°C using shallow angle X-ray diffraction. The glasses were reacted in SBF for time periods between 1 and 72 h prior to the experiment, allowing a detailed surface-sensitive analysis to be conducted on the evolution and growth of calcium phosphates and hydroxyapatite (HA) surface deposits. Thus, this experiment provides detailed X-ray diffraction data on the early stages of surface growth of calcium phosphates and HA. Furthermore, by varying the incident angle around the critical angle for external reflection it is possible to probe different depths of a given sample enabling some 3-D information to be gleaned.

2 Theory

For a material of density ρ g cm^{-3}, and an incident wavelength λ in Å, the critical angle, α_c, (in radians) is given by:

$$\alpha_c = 1.6 \times 10^{-3} \rho^{1/2} \lambda \quad (1)$$

For an incident angle $\alpha_i < \alpha_c$, the near surface region of the material will be illuminated to a depth z at which the electric field vector has fallen to $1/e$, where z is given by [12]:

$$z_{\alpha_i} < \alpha_c = \frac{\lambda}{2\pi(\alpha_c^2 - \alpha_i^2)^{\frac{1}{2}}} \quad (2)$$

Above α_c, penetration into the material increases rapidly with incident angle as shown in Fig. 1, where α_i is the incident angle and 2θ the scattering angle, z is the penetration depth into the sample, l is the path length into sample and l' is the scattered return path length exiting the sample. Refraction is negligible at the given energy thus $\alpha_i \approx \alpha_i'$ and $2\theta \approx 2\theta'$. For small incident angles (0.2–1.6°) the incident path length $l \gg l'$ compared to the relatively large scattering angles (20–40°), l' can therefore be neglected as well. It therefore follows that the penetration depth, z, is related to the incident angle by

$$z = l \sin(\alpha_i) \quad (3)$$

at small angles $\sin(\alpha_i) \approx \alpha_i$, and at the critical penetration depth, where the intensity falls to $1/e$ of the incident intensity, $l\mu = 1$, where μ is the (wavelength dependent) linear attenuation coefficient given by the product of the mass attenuation coefficient and the density. It therefore follows that if α_i is larger than α_c but still small we have

$$z_{\alpha_i} > \alpha_c = \frac{\alpha_i}{\mu} \quad (4)$$

For Bioglass® with a density 2.7 g cm^{-3}, at an incident X-ray wavelength of 1.0 Å, $\alpha_c = 2.63$ mrad (0.151°) and $\mu = 44.7$ cm^{-1}. Octacalcium phosphate, with a density 2.61 g cm^{-3} [6] has $\alpha_c = 2.58$ mrad (0.148°) and $\mu = 56.6$ cm^{-1}. Penetration depths for $\alpha_i > \alpha_c$, calculated using Eq. 4, are given in Table 1.

Table 1 Penetration depth for X-rays of wavelength 1.0 Å incident at an angle $\alpha_i > \alpha_c$ onto Bioglass® and octacalcium phosphate

Incident angle, α_i, (°)	Penetration depth, z, (μm)	
	Bioglass®	Octacalcium phosphate
0.2	0.8	0.6
0.5	2.0	1.5
1.0	3.9	3.1
1.6	6.2	4.9

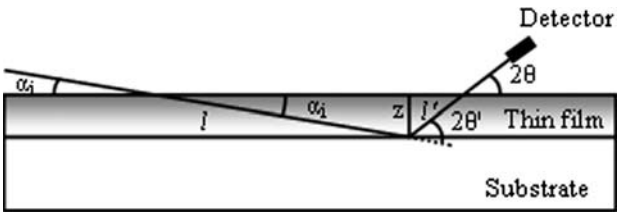

Fig. 1 Schematic of the shallow angle of incident X-ray diffraction

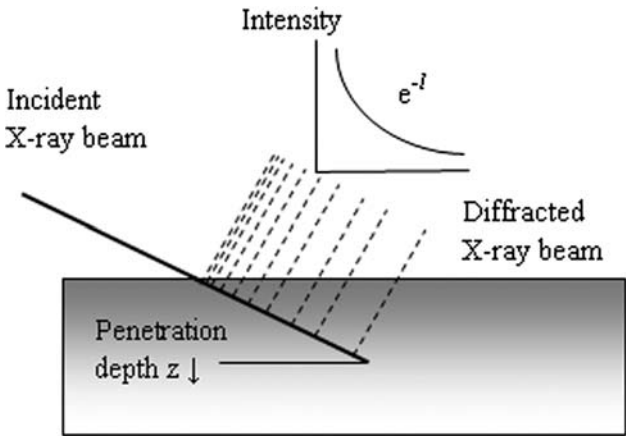

Fig. 2 X-ray path through the sample. The intensity of the scattered beam is proportional to e^{-l}, where l is related to the penetration depth as given by Eq. 3

The total X-ray intensity diffracted by a layer of thickness δ, taking into account absorption only, can be determined as shown in Fig. 2. It is therefore possible to calculate the thickness of a given layer by comparing the relative intensity expected from that layer with the calculated intensity anticipated from the underlying Bioglass® sample.

3 Experimental procedures

3.1 Sample preparation

Sodium carbonate (Na_2CO_3) and calcium carbonate ($CaCO_3$) were mixed together with ammonium dihydrogen phosphate ($NH_4H_2PO_4$) and silica (SiO_2) powder in the appropriate quantities to form $(CaO)_{26.9}(Na_2O)_{24.4}(SiO_2)_{46.1}(P_2O_5)_{2.6}$; also referred to as 45S5 Bioglass®. The powders were heated at 10°C per minute to 1370°C, equilibrated for 90 min before quenching into a preheated (350°C) carbon graphite mould. The samples were annealed at 350°C overnight before being allowed to cool slowly to room temperature. The samples were (dry) ground and polished to a three micron finish before immersing into simulated body fluid, a standard salt solution, at 37°C; preparation details of SBF are given by [13, 14]. After reacting in SBF the samples were removed and rinsed with distilled water and acetone to remove any residual salts and halt reactions. The SBF-reacted samples were then dried at 60°C overnight and stored in a desiccator until required.

3.2 Shallow angle X-ray scattering

The small angle X-ray scattering, SAXS, experiments were carried out using station 9.1 at the Daresbury Laboratory Synchrotron Radiation Source (SRS), UK using an incident wavelength of 1.0 Å. The longer wavelength was selected primarily to reduce the penetration depth (Eq. 3) thus ensuring that only the surface layers were measured.

The intrinsically highly parallel nature of the beam provided by a synchrotron radiation source is a key advantage over conventional focused laboratory X-ray sources for the shallow angle technique in that the associated geometric aberration effects are avoided. Furthermore, the high intensity beam provided by a synchrotron source is necessary for the relatively weak, diffuse scattering from the small volume of disordered material sampled in the shallow angle geometry.

The conventional (transmission) X-ray diffraction arrangement was modified to produce the shallow angle configuration. A narrow incident beam of 100 μm (H) by 10 mm (W) was used to reduce the footprint and limit contamination from the straight-through beam at the lowest incident angles. For shallow angle diffraction, the sample is set at a fixed, small angle α_i to the incident X-rays. Determination of the zero angle, θ_0, for samples mounted on the diffractometer is critical given the small angles used in data collection. To optimise θ_0 the intensity of the incident beam is first measured without a sample being present. The sample is then raised into the beam until the intensity drops by a factor of two. The sample is then rocked about θ until the intensity is maximised. This procedure of height and angle adjustment is repeated iteratively until the intensity at the centre of the rocking curve is half of the incident beam. It is also essential that the sample is smooth and flat; any significant irregularity in the film thickness will produce an uncertainty in α_i and hence on the collected scattering profile. The cast samples were 50 mm long to ensure that the samples covered the large footprint of the incident beam and the detectors were collimated to ensure scattering was only detected from regions of sample illuminated by the incident beam. The data was collected over the range $10° < 2\theta < 40°$, beyond 40° the scattered intensity and features were too weak to be analysed robustly.

Diffraction patterns were measured at incident angles of 0.2, 0.5, 1.0 and 1.6° for the Bioglass® samples which had been reacted in SBF for 1, 4, 8, 24 and 72 h, together with an unreacted sample for reference. The broad amorphous features generated during the initial reaction stages are difficult to quantify, the samples were therefore also heated at 650°C for 12 h and then re-measured in order to help determine the nature of the mineral deposits and underlying crystalline phases.

4 Results and discussion

Figure 3a–c show the shallow angle diffraction data for Bioglass® as a function of incident angle. Increasing the incident angle increases the penetration depth as shown in Table 1. It can therefore be seen that there is no noticeable change in structure between the surface and bulk of un-reacted Bioglass® (Fig. 3a) and that the structure is dominated by a single broad amorphous feature ~ 2.2 Å^{-1}. The broad amorphous feature ~ 2.2 Å^{-1} represents the structure of bulk Bioglass® and is in good agreement with the first peak position of Bioglass® determined by high energy X-ray diffraction [9] as shown in Fig. 3a (inset). The present data has been scaled to account for the number of scatterering centres in the beam.

Bioglass® reacted in SBF for 24 h shows a second amorphous feature ~ 1.6 Å^{-1}. At shallow angles of incidence the intensities of the two amorphous phases are approximately equal in magnitude. At higher incident angles (1.6°), where the X-rays penetrate further into the

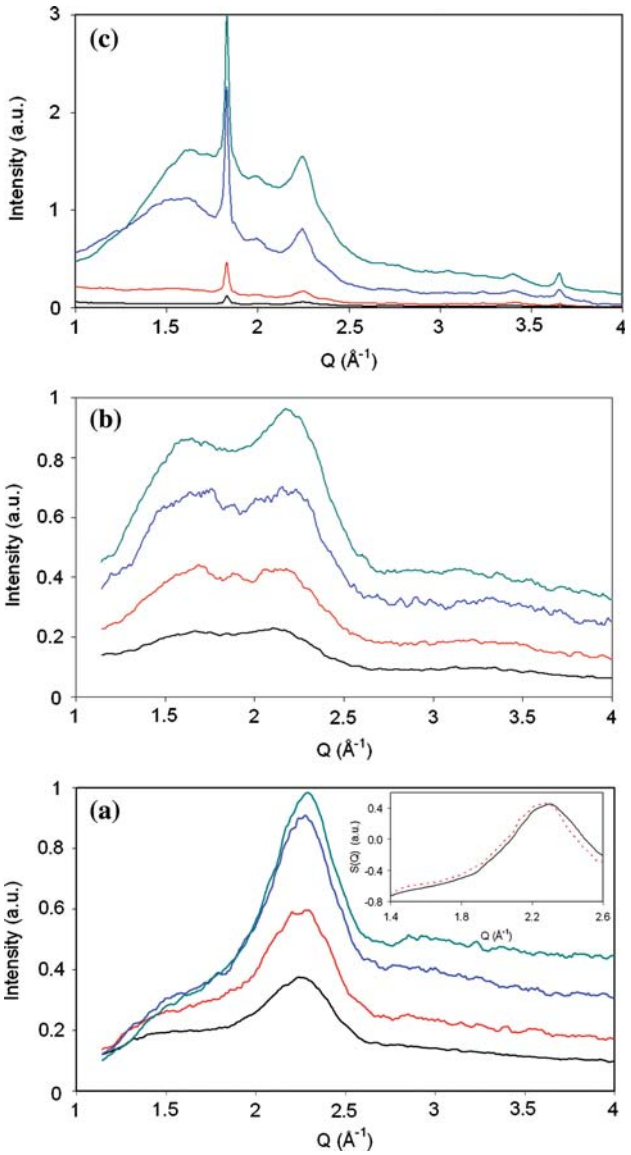

Fig. 3 The diffraction pattern of Bioglass® as a function of incident angle for **a** unreacted Bioglass®; the inset shows the diffraction pattern for the unreacted Bioglass® compared to the pattern obtained by FitzGerald et al [7] using conventional high energy X-ray diffraction, **b** Bioglass® reacted in SBF for 24 h and **c** Bioglass® reacted in SBF for 3 days. The incident angle 1.6°, 1.0°, 0.5° and 0.2° are given from top to bottom

bulk structure, the broad feature 2.2 Å^{-1} begins to dominate.

Figure 3c shows the shallow angle data for Bioglass® reacted in SBF for 3 days; the diffraction pattern is dominated by a large Bragg peak at 1.82 Å^{-1} with smaller peaks at 2.25, 3.4 and 3.64 Å^{-1}. These peaks are attributed to hydroxyapatite, with preferential orientation. The peaks at 1.82 Å^{-1} and 3.64 Å^{-1} are representative of the *(002)* and (*004*) reflections. The slightly broader Bragg peak at 2.25 Å^{-1} is a combination of the (*121*), (*211*) and (*112*) reflections, note the (*121*) reflection is the strongest naturally occurring reflection for HA. The Bragg peaks are present for all angles of incidence and mask the broad amorphous feature at ~2.2 Å^{-1} associated with the underlying bulk Bioglass®. The broad feature at ~1.6 Å^{-1} is only present at larger angles of incidence which suggests that crystallisation occurs at the SBF/amorphous calcium phosphate interface and not at the amorphous calcium phosphate/Bioglass® glass interface. This is further supported by the relatively flat backgrounds at shallow angles (0.2° and 0.5°) suggesting the amorphous contribution is negligible at the surface. For larger angles of incidence (1° and 1.6°), where the penetration depth is greater and scattering occurs from deeper within the sample, the broad amorphous feature centred at 1.6 Å^{-1} dominates the diffraction pattern. Therefore the amorphous calcium phosphate must form between the bulk Bioglass® and the outer crystalline surface. The preferred orientation of the hydroxyapatite in the (*001*) plane has previously been observed during the formation of hydroxyapatite [15, 16].

Figure 4 shows the shallow angle data for Bioglass®, reacted in SBF for various times, collected at a fixed incident angle of 1.6°. The evolution of an amorphous phase ~1.6 Å^{-1} is clearly evident; the feature is initially

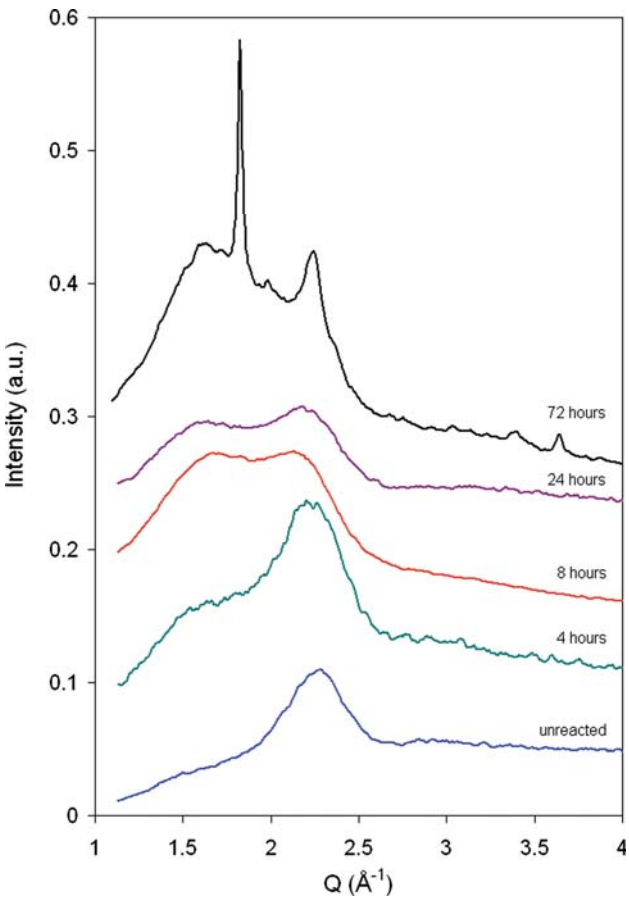

Fig. 4 The diffraction pattern of Bioglass® reacted in SBF for varying periods of time. All data sets were collected with an angle of incidence of 1.6°

identifiable as a small shoulder after only 4 h and by 8 h this feature is approximately equal in magnitude to the amorphous feature at 2.2 $Å^{-1}$ associated with unreacted Bioglass®. There appears to be little change in the relative intensities of the two amorphous phases at 1.6 and 2.2 $Å^{-1}$, which are approximately equal in magnitude, for samples reacted for 8 and 24 h in SBF. After 3 days reacting in SBF the amorphous phase $\sim$1.6 $Å^{-1}$ begins to dominate and there is evidence of crystallisation.

Diffraction patterns for the heat treated Bioglass® samples (650°C for 12 h) are given in Fig. 5; data were collected at a fixed incident angle of 1.6°. The unreacted Bioglass® (b) and 4 h reacted sample (c) both show a simple crystalline structure associated with bulk Bioglass® which is represented by $Na_6Ca_3Si_6O_{18}$ (a) [17]. The 24 h reacted sample (d) is still dominated by Bragg peaks associated with Bioglass® with the addition of a number of tiny Bragg peaks. The sample reacted in SBF for 3 days after heat treating shows a complex crystalline pattern (Fig. 5f) containing $Na_6Ca_3Si_6O_{18}$ associated with Bioglass® and Hydroxyapatite (e) [18].

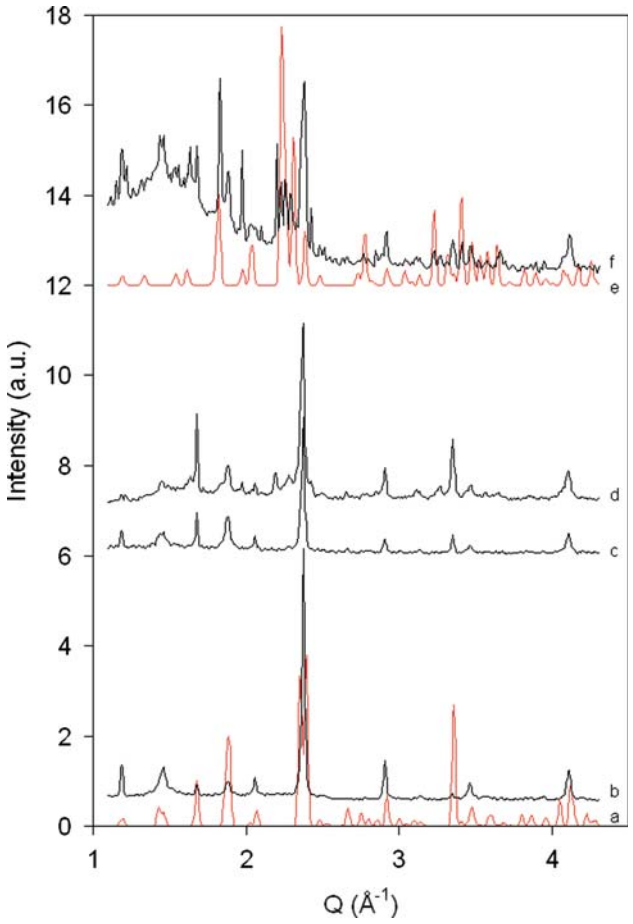

Fig. 5 The diffraction pattern of Bioglass® reacted in SBF for 0, 4, 24 and 72 h followed by heat treating at 650°C are given by *b*, *c*, *d* and *f* respectively. The diffraction pattern of $Na_6Ca_3Si_6O_{18}$ [15] and hydroxyapatite [16] are given by *a* and *e* respectively. All data sets were collected with an angle of incidence of 1.6°

It is also possible to estimate the thickness of the phosphate layer by taking into account the absorption and the relative intensities of the Bioglass® feature at 2.2 $Å^{-1}$ and the phosphate feature $\sim$1.6 $Å^{-1}$. Note, the form factors of Bioglass® at 2.2 $Å^{-1}$ and octa-calcium-phosphate at 1.65 $Å^{-1}$ are 8.1 and 7.4 respectively, and the number densities are 0.075 and 0.088 $Å^{-3}$. Thus taking the relative intensities of the phosphate and Bioglass® features leads to $\sim$7% discrepancy which is accounted for in the errors. The relative intensities of phosphate scattering for the sample reacted in SBF for 24 h are 45% and 55% at 1.6° and 1.0° incident angle respectively. This corresponds to estimated film thicknesses of 3.25 μm and 3.05 μm. It is not possible to estimate the thickness after 3 days since there is insufficient penetration into the Bioglass® to generate useful ratios, also the addition of the HA Bragg peak at 2.25 $Å^{-1}$ is in the middle of the amorphous Bioglass® feature. It is estimated that after 4 h reacting in SBF the film is $\sim$2 μm thick and by 8 h the thickness has increased to $\sim$4 μm. This therefore suggests that not only has the formation of ACP and HA rapidly decreased between 8 and 24 h but that some of the deposited layer may be re-dissolved into the SBF solution. It has been noted in previous studies on bioactive glasses [7] that after a short induction time crystallisation occurs but then some material re-dissolves with time.

It is worth noting that the surface texture has an important effect on the rate of hydroxyapatite formation. Induction times for apatite nucleation decrease as the surface area increases [19]. The shallow angle technique requires a flat polished surface in order to determine the incident angle as discussed above. The rate of nucleation and HA growth may therefore be reduced by the 3 μm polished surface.

5 Conclusions

The evolution of amorphous calcium phosphate and hydroxyapatite onto Bioglass® reacted in SBF has been studied using surface sensitive shallow angle X-ray diffraction. Amorphous calcium phosphate is detected for samples after only 4 h reacting in SBF. After 8 h reacting in SBF the intensity of the phosphate is comparable to the underlying signal from the bulk Bioglass®. There appears little change in the relative intensities of the calcium phosphate surface layer and the bulk Bioglass® between 8 and 24 h suggesting the surface formation slows dramatically during this time. It appears that the intensity of phosphate has actually decreased during this time suggesting part of the initial surface formation is re-dissolved

back into the SBF solution. Bragg peaks are clearly evident for samples reacted in SBF for 3 days. The crystallisation, attributed to hydroxyapatite, occurs on the surface of the amorphous calcium phosphate layer and not at the Bioglass® interface.

Acknowledgements The authors thank the EPSRC for financial support (Grant no. EP/E050611/1) SRS for beam time allocation, Dr. Tony Bell for assistance on station 9.1 and acknowledge use of the Chemical Database Service.

References

1. L.L. Hench, R.J. Splinter, W.C. Allen, T.K. Greenlee, J. Biomed. Mater. Res. **5**(6), 117 (1971). doi:10.1002/jbm.820050611
2. A.E. Clark, L.L. Hench, H.A. Paschall, J. Biomed. Mater. Res. **10**, 161 (1976). doi:10.1002/jbm.820100202
3. L.L. Hench, J. Wilson, D.C. Greenspan, J. Aust. Ceram. Soc. **40**, 1 (2004)
4. L.L. Hench, J. Mater. Sci. Mater. Med. **17**, 967 (2006). doi:10.1007/s10856-006-0432-z
5. See www.novabone.com and www.novamin.com for commercial details
6. S.V. Dorozhkin, M. Epple, Angew. Chem. Int. Ed. **41**, 3130 (2002). doi:10.1002/1521-3773(20020902)41:17<3130:AID-ANIE3130>3.0.CO;2-1
7. R.J. Newport, L.J. Skipper, D. Carta, D.M. Pickup, F.E. Sowrey, M.E. Smith, P. Saravanapavan, L.L. Hench, J. Mater. Sci. Mater. Med. **17**, 1003 (2006). doi:10.1007/s10856-006-0436-8
8. L.J. Skipper, F.E. Sowrey, R. Rashid, R.J. Newport, Z. Lin, M.E. Smith, Phys. Chem. Glasses **46**(4), 372 (2005)
9. V. FitzGerald, D.M. Pickup, D. Greenspan, G. Sarkar, J.J. Fitzgerald, K.M. Wetherall, R.M. Moss, J.R. Jones, R.J. Newport, Adv. Funct. Mater. **17**, 3746 (2007). doi:10.1002/adfm.200700433
10. V. FitzGerald, D.M. Pickup, D. Carta, D. Greenspan, R.J. Newport, Phys. Chem. Glasses **48**, 340 (2007)
11. V. FitzGerald, D.M. Pickup, D. Greenspan, K.M. Weatherall, R.M. Moss, J.R. Jones, R.J. Newport, Phys. Chem. Glasses (2008) (in press)
12. J.S. Rigden, R.J. Newport, G.J. Bushnell-Wye, J. Mater. Res. **12**, 264 (1997). doi:10.1557/JMR.1997.0034
13. T. Kokubo, H. Kushitani, S. Sakka, T. Kitsugi, T. Yamamuro, J. Biomed. Mater. Res. **24**(6), 721 (1990). doi:10.1002/jbm.820240607
14. International standard: ISO/FDIS 23317:2007
15. I. Rehman, J.C. Knowles, W. Bonfield, J. Biomed. Mater. Res. **41**(1), 162 (1998). doi:10.1002/(SICI)1097-4636(199807)41:1<162:AID-JBM19>3.0.CO;2-P
16. V. FitzGerald, R.A. Martin, J.R. Jones, D. Qiu, K.M. Wetherall, R.M. Moss, R.J, Newport, J. Biomed. Mater. Res. A (in press). doi:10.1002/jbm.a.32206
17. H. Ohsato, I. Maki, Y. Takeuchi, Acta Crystallogr. C **41**, 1575 (1985). doi:10.1107/S0108270185008617
18. L. Stork, P. Mueller, R. Dronskowski, J.R. Ortlepp, Z. Kristallogr. **220**, 201 (2005). doi:10.1524/zkri.220.2.201.59118
19. M.M. Pereira, A.E. Clark, L.L. Hench, J. Am. Ceram. Soc. **78**(9), 2463 (1995). doi:10.1111/j.1151-2916.1995.tb08686.x